Available online at www.sciencedirect.com
ScienceDirect
International Journal of Multiphase Flow 32 (2006) 996–1016
International Journal of Multiphase Flow
www.elsevier.com/locate/ijmulflow

Three-dimensional flow pattern visualization and bubble size distributions in stationary and transient upward flashing flow

A. Manera [a,b,*], H.-M. Prasser [a], D. Lucas [a], T.H.J.J. van der Hagen [b]

[a] Forschungszentrum Rossendorf e.V. (FZR), Institute of Safety Research, P.O.B. 510119, D-01324 Dresden, Germany
[b] Interfaculty Reactor Institute, Delft University of Technology, Delft, The Netherlands

Received 14 October 2004; received in revised form 18 March 2006

Abstract

For the first time, an experimental three-dimensional reconstruction and visualization of stationary and transient flashing flow in a vertical pipe (47 mm diameter) is presented. The measurements have been performed by means of wire-mesh sensors. This type of sensor delivers two-dimensional void-fraction distributions in the pipe cross-section where it is mounted with a maximum sampling rate of 10,000 frames per second. A sampling rate of 1200 frames per second has been used in this work. Steam bubbles have been identified from the wire-mesh data and their complete three-dimensional reconstruction has been performed by taking into account the steam bubble velocity. For the estimation of the bubble velocity, two wire-mesh sensors positioned at a small axial distance from each other have been used. The velocity has been determined by cross-correlation of the two wire-mesh signals, by direct identification of the traveling time of the steam bubbles between the two sensors and by means of a drift-flux model. A comparison between the three methods of bubbles velocity measurement is reported. Stationary and time-dependent bubble size distributions have been derived. The stationary radial void-fraction profiles have been decomposed according to bubble size classes and compared with the results obtained with an equilibrium model.

Keywords: Flashing; Two-phase flow; Three-dimensional visualization; Bubble size

1. Introduction

Flashing flows in vertical pipes have found great interest in the last years because of importance during the start-up phase of natural-circulation-cooled Boiling Water Reactors (BWRs). In these systems the coolant

* Corresponding author. Address: Forschungszentrum Rossendorf e.V. (FZR), Institute of Safety Research, P.O.B. 510119, D-01324 Dresden, Germany. Tel.: +49 351 260 2502; fax: +49 351 260 2383.
E-mail address: annalisa.manera@colenco.ch (A. Manera).

0301-9322/$ - see front matter
doi:10.1016/j.ijmultiphaseflow.2006.03.005

flow is driven by natural circulation and a long adiabatic section (riser or chimney) is present above the reactor core to enhance the flow rate.

It has been demonstrated theoretically (Inada et al., 2000; Van Bragt et al., 2002) and experimentally (Wissler et al., 1956; Aritomi et al., 1992; Furuya et al., 1995; Manera and van der Hagen, 2003; Manera, 2003) that, under specific conditions, flashing occurring in the adiabatic section may trigger undesired self-sustained flow oscillations. To avoid such instabilities, optimal start-up procedures are needed. Such procedures are tested by means of so-called best-estimate codes (TRACG, ATHLET, RELAP, etc.). These codes are based on the one-dimensional two-fluid model approach and necessitate a set of constitutive relations to couple the balance equations for the liquid and vapour phase. These relations have not been derived specifically for flashing flow in vertical pipes subsequent to a decrease of gravitational head. As a matter of fact, computer simulations (Andersen et al., 1995; Cheng et al., 1998b; Paniagua et al., 1999; Cheung and Rao, 2000; Tiselj and Cerne, 2000; Analythis and Lübbesmeyer, 2002; Sengstag, 2002) of natural circulation BWRs systems at low pressure (when the flashing phenomenon plays a key-role) have often given unsatisfactory and sometimes even contradictory results.

Knowledge of the characteristics of flashing flows is therefore of fundamental importance for the determination and assessment of models to be implemented in best-estimate codes for the design of optimal start-up procedures for the natural circulation BWRs (and in general of natural circulation two-phase flow systems).

The experiments and models available in literature (Riznic and Ishii, 1989; Domnick and Durst, 1995; Downar-Zapolski et al., 1996; Elias and Chambrè, 2000; Hahne and Barthau, 2000) mainly refer to flashing in horizontal pipes as a consequence of sudden depressurization (i.e. blow down transients, for instance due to a pipe rupture) or close to a pipe restriction and cannot be directly applied to flashing flows in vertical pipes caused by variations of gravitational pressure head.

Experimental studies on two-phase flow in vertical pipes are reported in literature, but mainly refers to air–water flows, in which air and liquid are supplied separately, and scarce literature can be found focused on steam–water flows in which the steam is produced by heaters placed below an adiabatic test section. Very little is known about flashing flows, in which steam is produced in the super-heated liquid due to a decrease of the gravitational head along the system.

Objective of the present paper is to analyze the three-dimensional structure of such flashing flows and investigate how the flow patterns compare with flow maps available in literature, to check whether models based on equilibrium of bubble forces can be applied for the prediction of bubbles radial distribution in flashing flows as well, and to study whether drift-flux models are suitable for applications to transient flashing flows. In this work, the structure of flashing flows caused by a decrease of gravitational head is studied for the first time, both in stationary and transient conditions. A three-dimensional visualization of the flow patterns is obtained for several flow conditions and a comparison with available flow map is presented. Advanced instrumentation, namely wire-mesh sensors, is used for this task. Unique experimental data have been obtained for bubble size distributions and their temporal evolution during transients. An equilibrium model, based on the balance of the forces acting on the bubbles, is successfully applied for the first time to predict bubbles radial distribution in flashing flow. In addition, the performances of the GE-ramp model are analyzed for the prediction of the time-dependent steam velocity during transient flashing. Such model was selected on the basis of previous work (Manera, 2003; Manera et al., 2003) regarding the suitability of drift-flux models to predict the void fraction during flashing flows.

2. The experimental set-up

The test facility (see scheme in Fig. 1) is a steam/water loop built at the Delft University of Technology to simulate the behavior of a natural-circulation BWR at low-pressure conditions. Demineralized water is used as working fluid. The test section consists of an insulated adiabatic pipe (3 m length, 47 mm diameter), so-called riser, made of glass, built on top of four parallel heated channels. The steam produced in the heated and in the adiabatic sections is condensed by a heat exchanger. The pressure can be set higher than the atmospheric pressure by means of a steam dome where liquid and steam are kept at saturation conditions (in this case the loop is pressurized by means of a pressure vessel containing air and water separated by a membrane. After the pressurization the vessel is disconnected from the loop). A buffer vessel is used to damp temperature oscillations at

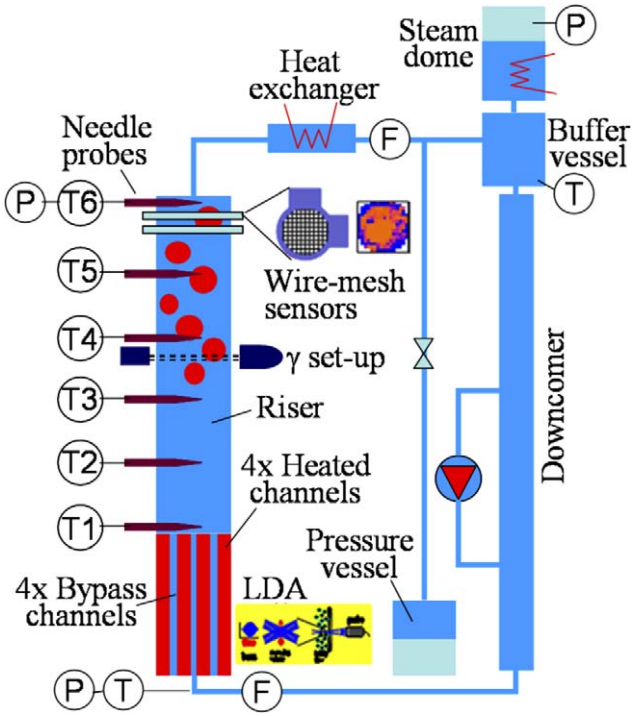

Fig. 1. Scheme of the test facility.

Table 1
Characteristics of the test facility

Power range per rod	0–3 kW
Pressure range	1–5 bar
Fuel channel diameter	20.4 mm
Fuel rod diameter	12.5 mm
Heated section length	1.95 m
Adiabatic section diameter	47 mm
Adiabatic section length	3 m

the outlet of the heat exchanger in order to ensure a constant temperature at the inlet of the heated section. The facility can be operated both in forced and natural circulation conditions. The main characteristics of the test facility are reported in Table 1.

The measurements presented in this paper have been carried out at atmospheric pressure. During each experiment, the power level and the temperature at the inlet of the heated section are kept constant.

2.1. Instrumentation

The instrumentation of the test facility is schematically illustrated in Fig. 1. The flow rate at the inlet of the heated section and before the steam dome is measured by means of magnetic flow-meters. Thermocouples are located at the inlet and outlet of each heated channel, along the adiabatic section, in the heat exchanger and in the steam dome. The temperature at the inlet of the heated section is measured by means of a PT100 for higher accuracy. Pressure sensors are used to measure the absolute pressure at the inlet of the heated section, at the outlet of the riser and in the steam dome. Differential pressure sensors are mounted across the steam dome (for water level measurements) and across the valves at the inlet of the heated section (such valves, not reported in

Fig. 1, are present at the inlet of each heated channels in order to control the inlet friction for each channel separately). Beside standard instrumentation, advanced measuring techniques are used for detailed void-fraction measurements and for velocity measurements at high sampling rate. The latter measurements are performed by means of Laser-Doppler Anemometry set-ups. The void-fraction measurements are performed by means of local conductivity needle-probes equidistantly distributed along the axis of the adiabatic section, and by wire-mesh sensors (Prasser et al., 1998). Two of such sensors are mounted in the upper part of the adiabatic section, positioned at an axial distance of 27.5 mm from each other. Details are given in the next paragraph. Further information about set-up and instrumentation is given by Manera (2003).

3. The wire-mesh sensor

The wire-mesh sensor, developed at the Forschungszentrum Rossendorf (FZR, Germany) allows the measurement of the instantaneous two-dimensional void-fraction distribution over the cross-section of a pipe. The measurement is based on the local instantaneous conductivity of the fluid flowing in the pipe. Details on the working principle of the sensors are given by Prasser et al. (1998).

The inner diameter of the two sensors used in the experimental set-up is 47 mm (equal to the inner diameter of the adiabatic section in which they are mounted). Each sensor consists of two electrode grids that are positioned perpendicularly to each other (see Fig. 2) in order to form a matrix of 16×16 crossing points. The distance between two successive parallel wires is 2.8 mm, this being the spatial resolution of the sensor. The sampling frequency of such a device can be set up to 10 kHz. A sampling frequency of 1200 Hz has been used in the present study. The wires have a diameter of 120 μm and occupy ~4% of the total cross-section, so that the flow resistance introduced by the sensor is not significant.

3.1. Treatment of the measured signal

The wire-mesh sensor delivers a matrix of 16×16 instantaneous local conductivity measurements at each wires crossing point. Defining a rectangular coordinate system having its origin in the center of the sensor, the temporal- and spatial-coordinates are expressed as

$$t = i \cdot \Delta t = \frac{i}{f_m}; \quad x = j \cdot \Delta x; \quad y = k \cdot \Delta y,$$

being Δt the sampling time, the spatial pitches $\Delta x = \Delta y = 2.8$ mm and the sampling frequency $f_m = 1200$ Hz.

Assuming a linear dependency between local instantaneous conductivity and void fraction—this assumption has been proven to be satisfactory in previous works (Prasser et al., 1998; Richter, 2001)—the local fluid

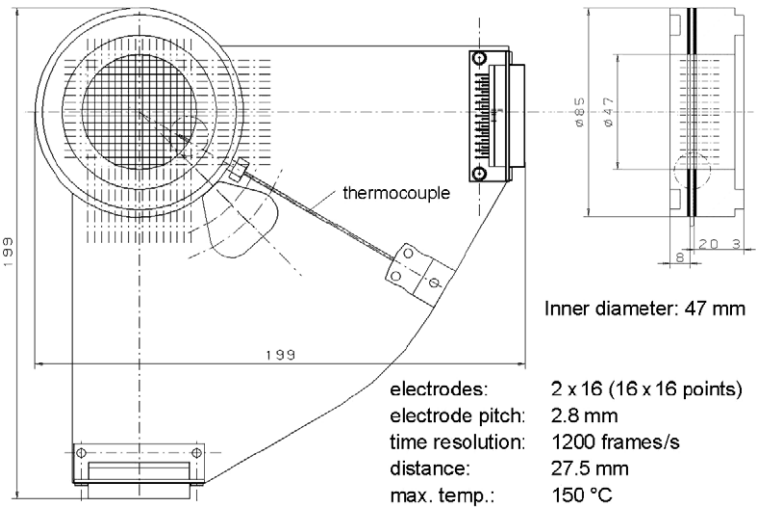

Fig. 2. Scheme of the wire-mesh sensor.

conductivity $u_{i,j,k}$ measured at the time instant $i\Delta t$ at the crossing point identified by the indexes j and k can be converted into void fraction $\varepsilon_{i,j,k}$ according to

$$\varepsilon_{i,j,k} = \frac{u_{i,j,k} - u_{\mathrm{G}_{j,k}}}{u_{\mathrm{L}_{j,k}} - u_{\mathrm{G}_{j,k}}} \tag{1}$$

where $u_{\mathrm{G}_{j,k}}$ and $u_{\mathrm{L}_{j,k}}$ are the fluid conductivity that would be measured if the area around the crossing point (j,k) would be completely filled with gas or liquid respectively. These data are retrieved during a calibration procedure in which measurements are performed in conditions of "tube completely filled with liquid" and "tube completely filled with gas". The data are stored for each of the 16×16 crossing points of the sensor.

A special correction is needed if the temperature of the fluid is expected to vary during the experiments. In this case a decrease (increase) of the liquid temperature will cause a decrease (increase) of the liquid conductivity u_{L} that would be interpreted as an increase (decrease) of void fraction, if the relation (1) is adopted. To take into account temperature variations, the liquid conductivity is measured by the wire-mesh sensor at different liquid temperatures and a linear regression is derived (Manera, 2003) for each crossing point (j,k). The fluid temperature is measured by means of a thermocouple positioned at the location of the wire-mesh sensor (see Fig. 2). The temperature correction results in the following relation:

$$\varepsilon_{i,j,k} = \frac{u_{i,j,k} - u_{\mathrm{G}_{j,k}}}{u^0_{\mathrm{L}_{j,k}} - u_{\mathrm{G}_{j,k}}} \frac{aT_0 + b}{aT + b} \tag{2}$$

where $u^0_{\mathrm{L}_{j,k}}$ is the liquid conductivity measured at the reference temperature T_0 and a and b are the coefficient of the linear regression.

As an example, the cross-section-averaged void fraction measured by the wire-mesh during a flashing-induced flow oscillation is shown in Fig. 3a. If the temperature variation is not taken into account (i.e. a constant liquid conductivity is assumed for the conversion from fluid conductivity to void fraction) the void fraction might exhibits also negative values during a flashing cycle, while it shows positive values between two successive flashing cycles even though only liquid is present in the riser. This is due to the fact that the liquid temperature varies in time and exhibits a local maximum during a flashing cycle and a local minimum between two successive cycles. Since the liquid conductivity decreases with decreasing temperature, a decrease (increase) of temperature is erroneously interpreted as an increase (decrease) of void fraction. The effect vanishes when the described temperature calibration is applied (see Fig. 3b).

Note that for the evaluation of the cross-section-averaged void fraction a weighting factor is needed to take into account whether the measurement area associated to a given crossing point (j,k) contributes completely (central meshes) or only partially (meshes at the periphery) to the pipe cross-section (Prasser et al., 1998).

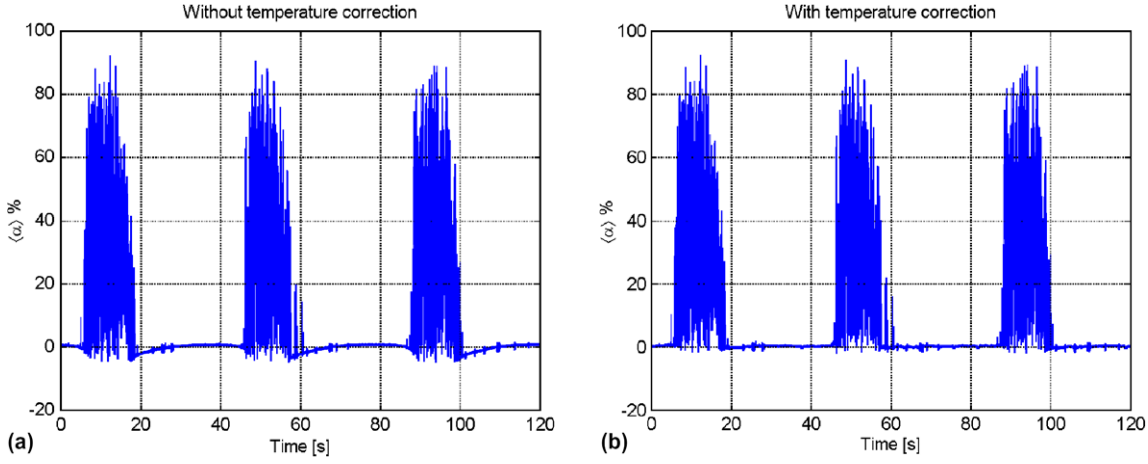

Fig. 3. Effect of temperature correction on void-fraction measurements.

Several studies have been performed to assess the error of this measurement technique on the void fraction. A comparison with a fast X-ray tomograph in air–water mixture at ambient temperature has shown that for bubbly flow the absolute error on the void fraction is lower than 1%, whereas for slug flow the maximum absolute value is found to be underestimated by less than 4% (Prasser et al., 2005a). The void-fraction under-estimation is caused by the formation of a liquid film between the steam bubbles and the wires of the sensor. Such effect disappears with increasing liquid temperature. Since the measurements presented in this paper are carried out on a steam/water mixture at atmospheric pressure, the absolute error on the void fraction is lower than 4%.

3.2. Bubble reconstruction algorithm

The algorithm used to identify bubbles starting from the wire-mesh signal has been developed by Prasser et al. (2001). Starting point of the algorithm is the three-dimensional matrix of local void-fractions ε_{ijk} measured by the wire-mesh sensor.

A bubble-object is defined as a region of connected elements (i,j,k) containing gas phase surrounded by elements containing liquid phase. Each element (i,j,k) belonging to the same bubble-object is associated with a common number (so-called bubble identifier n_B) that is unique for each bubble.

However, due to the finite size of the measuring volume, a sharp distinction between elements filled with gas or liquid phase cannot be obtained. As a matter of fact, the local void fraction ε_{ijk} can take all values between zero (liquid) and unity (steam), since it can happen that steam only partially covers the measurement area defined by two crossing wires. Moreover a certain level of noise has also to be taken into account. Consequently, a threshold ε_{MIN} has to be used to distinguish between gas- and liquid-containing elements (Prasser et al., 2001). Without such a threshold, bubbles very close to each other might be erroneously unified. On the other hand, a high threshold may lead to the division of a bubble into unrealistic fragments.

The algorithm for the bubble identification first searches for local void-fraction maxima ε_{MAX}. Then, for each of these maxima a recursive subroutine (FILL subroutine) is started to assign to all neighboring elements (i,j,k) belonging to the same bubble the same bubble identifier n_B (the flow chart of the subroutine is shown in Fig. 4). When the FILL procedure for the bubble n_B is terminated, the bubble identifier n_B is increased to the next integer value and the procedure is repeated until no new start-element can be found in the data array. Result of the algorithm is a three-dimensional array of elements b_{ijk} having the same dimensions as the void-fraction array and containing the identifier of the bubble to which the element (i,j,k) belongs. Before starting the FILL procedure, all the elements b_{ijk} are set to zero. In the case in which a given element

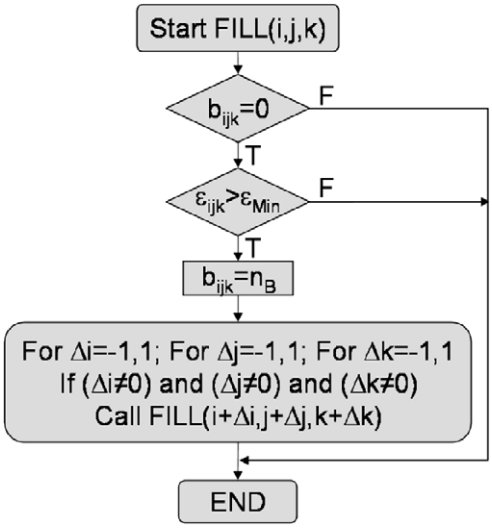

Fig. 4. Flow chart of the FILL subroutine for bubble identification.

(i,j,k) is occupied by liquid, the corresponding array element b_{ijk} is not assigned to any bubble, so that its value remains equal to zero. For local void fraction below the threshold ε_{MIN} the FILL subroutine is not executed. Prasser et al. (2001) have shown that an optimum is achieved when a differential threshold $\Delta\varepsilon_{LEVEL}$ is used to terminate the FILL procedure. In this case, the threshold ε_{MIN} is set equal to $\varepsilon_{MAX} - \Delta\varepsilon_{LEVEL}$.

The elements that surround bubbles and have not been assigned yet by the FILL subroutine (because their void fraction is lower than the threshold ε_{MIN}) are treated by means of an agglomeration algorithm that associates these elements to the bubbles that have already been identified. This subroutine does not create new bubble identifiers n_B. In the present work, a minimum value of 50% was chosen for the local void-fraction maxima ε_{MAX} that define a bubble element and the differential threshold $\Delta\varepsilon_{LEVEL}$ was set equal to 20%.

An example of the result of the bubble reconstruction algorithm is shown in Fig. 5. The two columns are derived from the lower and upper wire-mesh sensors respectively and represent virtual side cross-section views obtained by stacking one on top of each other the signals measured by each wire-mesh sensor along one pipe diameter at different time instants. Different colors are associated to different bubbles as identified by the bubble identification algorithm.

It is clear that for a complete three-dimensional reconstruction of the bubbles, the bubble velocity is needed. In first approximation, it can be assumed that all the elements (i,j,k) belonging to a given bubble move with the same velocity. For stationary flow it is generally assumed that the bubble velocity equals the gas superficial velocity divided by the cross-sectional-averaged void fraction. Unfortunately, the steam superficial velocity is not known a priori for steam–water flows because of the mass transfer between liquid and vapor phase (the mass transfer between phases is of particular importance in flashing flows). To overcome this problem, the steam velocity can be assessed by means of cross-correlation techniques based on local (Roy et al., 1994; Van Hout et al., 2001; Wang and Ching, 2001; Ohnuki and Akimoto, 2000) or cross-sectional-averaged (Costigan and Whalley, 1997; Cheng et al., 1998a; Hills et al., 1998; Mi et al., 2001) void-fraction signals. The latter method is used in this study.

Once the steam velocity w_G is known, the volume of a bubble can then be calculated as

$$V_B = w_G \Delta x \Delta y \Delta t \sum_{i,j,k \in B} \varepsilon_{i,j,k} \tag{3}$$

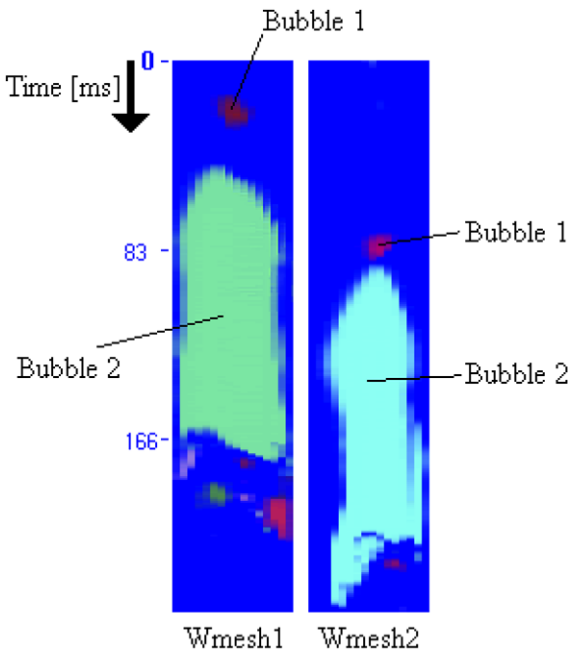

Fig. 5. Virtual sectional side views extracted from wire-mesh sensors data.

where B refers to the set of elements (i,j,k) belonging to the given bubble. The corresponding bubble equivalent diameter is calculated as

$$D_{\mathrm{eq,B}} = \sqrt[3]{\frac{6}{\pi} V_{\mathrm{B}}} \tag{4}$$

The soundness of the cross-correlation method, applied in the present work to estimate bubbles velocities, is demonstrated by Hills et al. (1998). They found that in case of bubbly flow the velocity extracted by cross-correlating the cross-sectional-averaged void-fraction signals is in very good agreement with the bubbles velocity. This is true also in case of cap bubbles and bubble clusters. For the slug-flow regime, where slugs and smaller bubbles are both present in the flow, Hills et al. (1998) demonstrated that the cross-correlation method gives the velocity of the slugs only. This happens because the slugs give a major contribution to the cross-sectional-averaged void fraction, while the contribution of smaller bubbles is negligible.

In view of the results obtained by Hills et al. (1998), the cross-correlation method applied in the present work gives an inexact estimation of the velocity of smaller bubbles in case of slug/churn flow regime. The error on the bubble velocity can be estimated applying the correlations given by Tomiyama (1998) and by Nicklin and Davidson (1962). The Tomiyama correlation applies to a wide range of bubbles diameters. For large bubbles (equivalent diameter larger than 0.63 times the pipe diameter) the influence of the pipe walls on the bubble velocity is considered by means of a correction factor. The correlation by Nicklin and Davidson describes the dependence of the velocity of slugs on the pipe diameter. The maximum difference between the slugs and bubbles drift velocities obtained by these correlations occurs for bubble sizes around 2 mm and amounts to about 10%. The error of the absolute velocity is in reality smaller than 10% since the bubbles move in an upward flowing liquid phase. The concomitant error of the bubbles equivalent diameter is up to of about 3%, since it is proportional to the one third power of the bubble velocity.

4. Three-dimensional flow visualization

As mentioned in Section 3.2, once the bubble velocity is known it is possible to transform the time coordinate in the spatial coordinate perpendicular to the measurements plane. To visualize the three-dimensional array of instantaneous local void fractions delivered by the wire-mesh sensors a simplified ray-tracing algorithm is used (Prasser et al., 2005b).

Lets suppose that white light arrives from one side of the pipe in direction parallel to the x-axis, as schematically illustrated in Fig. 6, and that the observation is performed from the direction parallel to the y-axis.

Indicating with Φ_x the vector of light intensity, the boundary conditions at the pipe wall $x = 0$ ($j = -n_{\mathrm{el}}/2$ in the discrete coordinate system, where n_{el} specifies the number of wire-mesh electrodes) can be written as

$$\vec{\Phi}_{x_{j=0,k}} = \vec{\Phi}_{\mathrm{white}} = (\varphi_{\mathrm{red}_{\mathrm{white}}}, \varphi_{\mathrm{green}_{\mathrm{white}}}, \varphi_{\mathrm{blue}_{\mathrm{white}}}) \tag{5}$$

On each point of the measurement domain, the light intensity vector Φ_x will have three components quantifying the red, green and blue content of the incident light. These components will be partially absorbed when the light beam will propagate through the steam and liquid present in the column characterized by the matrix of void-fractions $\varepsilon_{i,j,k}$. To evaluate the light intensity in each point of the measurement plane, it is first necessary to define vectors of absorption coefficients Λ_{G} and Λ_{L} for the steam and the liquid phase respectively. These vectors represent the absorption coefficients for the three light components of red, green and blue. For a given time instant, at each point (j,k) of the measuring plane the light intensity becomes:

$$\vec{\Phi}_{x_{j,k}} = \vec{\Phi}_{x_{j-1,k}} \left[1 - \vec{\Lambda}_{\mathrm{G}} \varepsilon_{j,k} - \vec{\Lambda}_{\mathrm{L}} (1 - \varepsilon_{j,k})\right] \quad \text{for } j \geqslant -\frac{n_{\mathrm{el}}}{2} \quad \text{and} \quad j \leqslant \frac{n_{\mathrm{el}}}{2} \tag{6}$$

where $n_{\mathrm{el}}/2$ specifies the outer boundary of the measurements domain. Finally, to reconstruct the image, the intensity of the light that is scattered toward the observer (see Fig. 6) in the direction of the y-axis has to be calculated. For this aim, scattering coefficients Ω_{G} and Ω_{L} of steam and liquid respectively for the three light components are defined. The intensity of light that is scattered toward the observed (i.e. in the y-direction) at each point (j,k) is expressed by

$$\vec{Q}_{j,k} = \vec{\Phi}_{x_{j,k}} [\vec{\Omega}_{\mathrm{G}} \varepsilon_{j,k} - \vec{\Omega}_{\mathrm{L}} (1 - \varepsilon_{j,k})] \tag{7}$$

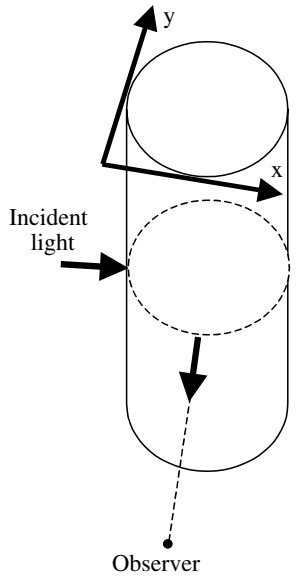

Fig. 6. Scheme for the 3D flow visualization.

This light will be partially absorbed while passing through the two-phase mixture in the y-direction. The light intensity Φ_y that travels in the y-direction will thus be a combination of source terms and absorption:

$$\vec{\Phi}_{y_{j,k}} = \vec{\Phi}_{y_{j,k-1}}\left[1 - \vec{\Lambda}_{\mathrm{G}}\varepsilon_{j,k} - \vec{\Lambda}_{\mathrm{L}}(1-\varepsilon_{j,k})\right] + \vec{Q}_{j,k} \quad \text{for } k \geqslant -\frac{n_{\mathrm{el}}}{2} \quad \text{and} \quad k \leqslant \frac{n_{\mathrm{el}}}{2} \tag{8}$$

with "black" as initial value:

$$\vec{\Phi}_{y_{j,k=0}} = \vec{\Phi}_{\mathrm{black}} = (\varphi_{\mathrm{red}_{\mathrm{black}}}, \varphi_{\mathrm{green}_{\mathrm{black}}}, \varphi_{\mathrm{blue}_{\mathrm{black}}}) \tag{9}$$

The value of Φ_y found for $k = n_{\mathrm{el}}/2$ represents the light intensity that reaches the observer. The above described procedure is repeated for successive time frames i. The three dimensional flow visualization is obtained by plotting one below each other in the vertical direction the vector $\vec{\Phi}_{y_{j,k}}$ calculated for $k = n_{\mathrm{el}}/2$ at each time instant $i\Delta t$. The vertical axis of the image is scaled by means of the steam velocity. A time-dependent steam velocity can be considered as well.

A clear advantage of the described method is a more realistic picture of the three-dimensional flow pattern that contains information of the entire three-dimensional void-fraction distribution. Such information would be lost if only a virtual sectional side view (as the one shown in Fig. 5) along the axis of the pipe is shown.

5. Stationary flashing flow

A series of experiments was performed at atmospheric pressure in condition of forced circulation (Manera, 2003; Manera et al., 2003) (see Table 2 for the measurements conditions). The use of forced circulation was necessary to ensure a constant flow rate at the inlet of the test section for a wide range of operating conditions. This in view of the fact that, as mentioned in the introduction, a natural-circulation two-phase system may exhibit flow oscillations when operated at low pressures. Data from the wire-mesh sensors were recorded for 200 s. From the series, two sets of measurements are selected at constant superficial liquid velocity and increasing superficial vapor velocity to be discussed here. The main variables are reported in Table 2. The last column in the table indicates the distance in length over pipe-diameter between the measurement points (where the lowest wire-mesh sensor is located) and the lowest axial location at which flashing occurs (flashing front). Below the flashing front, flashing does not propagate in the liquid bulk. The temperature at the inlet of the heated section T_{inl}, the power and the superficial liquid velocity J_{L} are the controlling parameters of the experiments. The superficial steam velocity J_{G} is determined a posteriori as the product of the steam bubble velocity

Table 2
Measurements in forced circulation conditions

	T_{inl} (°C)	Power (kW)	J_L (m/s)	J_G (m/s)	L/D Flashing front
SET 1					
A1	92	8.80	0.11	0.005	0.5
B1	92	9.12	0.11	0.030	4
C1	92	9.84	0.11	0.240	15
D1	92	10.4	0.11	0.590	32
E1	92	10.9	0.11	0.830	54
SET 2					
A2	96.2	7.20	0.14	0.018	1
B2	96.6	7.60	0.14	0.627	17
C2	96.4	7.88	0.14	0.775	28
D2	96.4	8.20	0.14	0.902	34
E2	96.6	8.64	0.14	1.100	52
F2	96.8	8.96	0.14	1.270	54

obtained by means of cross-correlation techniques and the cross-section-averaged void fraction measured by means of the lower wire-mesh sensor.

The visualization of the flow pattern obtained with the technique described in the previous paragraph is shown in Fig. 7 for the two sets of experiments described in Table 2. The picture is scaled such that the length of the column is 20 times the pipe diameter ($20 * 47 = 940$ mm). The flow pattern transits from bubbly to slug flow when the superficial vapor velocity increases.

The corresponding distributions of bubble length and equivalent diameter are presented in Figs. 8 and 9 respectively. The equivalent diameter is calculated according to Eq. (4). To evaluate the bubble length, first the time instants $t_{B,front}$ and $t_{B,back}$ at which the front and the back of the bubble touch the wire-mesh sensor are determined. The bubble length is then calculated as the product of the steam velocity and the time interval ($t_{B,back} - t_{B,front}$). The distributions represent the part of the void fraction that is carried by bubbles of a given length or equivalent diameter. In this way, the area under the distribution gives the cross-section-averaged void fraction $\langle\varepsilon\rangle$. The class width for calculating these histograms was 0.5 mm for bubbles length/equivalent diameter lower than 10 mm. For larger bubbles the class width was increased exponentially. This was necessary to achieve smooth distributions because large bubbles are rare but carry a large quantity of void.

In Fig. 8 the flow pattern is indicated for each case according to the Mishima–Ishii flow map (Mishima and Ishii, 1984). Confronting the predicted flow pattern with the visualization presented in Fig. 7 good agreement is found. This finding is quite remarkable since the Mishima–Ishii flow map has not been developed for flashing flow and in particular for flows where void production takes place along the test section. In this specific case it is not possible to define a development length as for the air–water experiments where a constant air flow is injected in the test section or as for the steam–water experiments in which steam is produced by heaters below an adiabatic test section and no further production of steam takes place in the test section itself. Analyzing Figs. 8 and 9 it can be seen that the transition from bubbly to slug flow is characterized by the well known transition from unimodal to bimodal bubbles size distribution.

The unimodal distribution exhibits a tail toward lower bubbles sizes when cap bubbles are present in the flow. An increase of superficial steam velocity gives rise to longer Taylor bubbles, while an increase of the superficial liquid velocity yields shorter Taylor bubbles.

5.1. Void-fraction profile and decomposition according to bubble-size classes

Tomiyama and co-workers (Tomiyama et al., 1995, 1999) stated that for a bubble radius corresponding to a critical modified Eötvös number given by

$$Eo_{mod} = \frac{g(\rho_L - \rho_G)}{\sigma} d_{xy}^2 \tag{10}$$

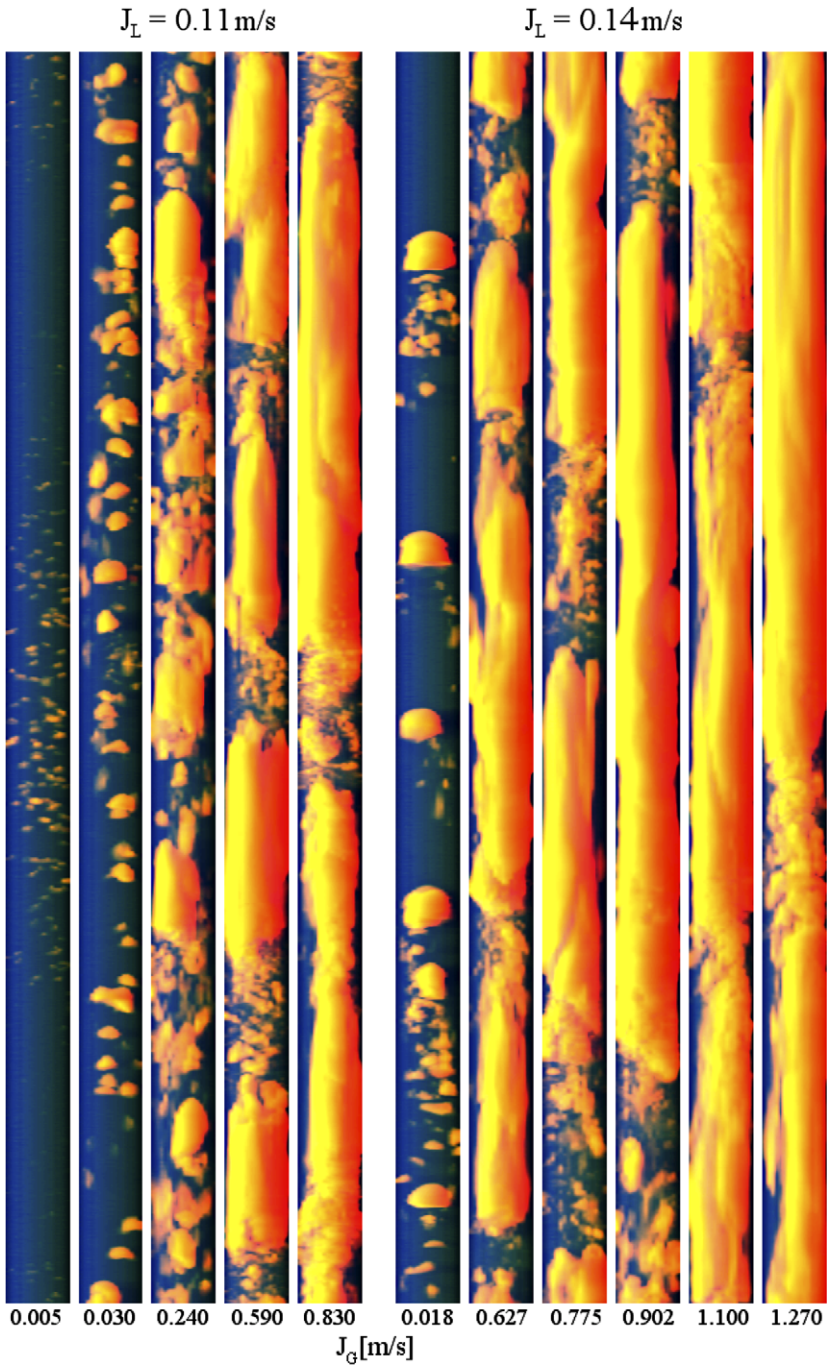

Fig. 7. Series of flow-pattern visualizations at constant liquid superficial velocity and increasing steam superficial velocity. The columns have a length of 20 times the pipe diameter, the latter being 47 mm.

an inversion of the direction of the lift force occurs, which pulls the bigger bubbles toward the center of the pipe. In the formula above d_{xy} represents the maximum bubble diameter in the cross-section. In case of steam/water mixture at atmospheric pressure the critical equivalent bubble diameter (evaluated from the bubble volume assuming spherical shape) is about 5.36 mm.

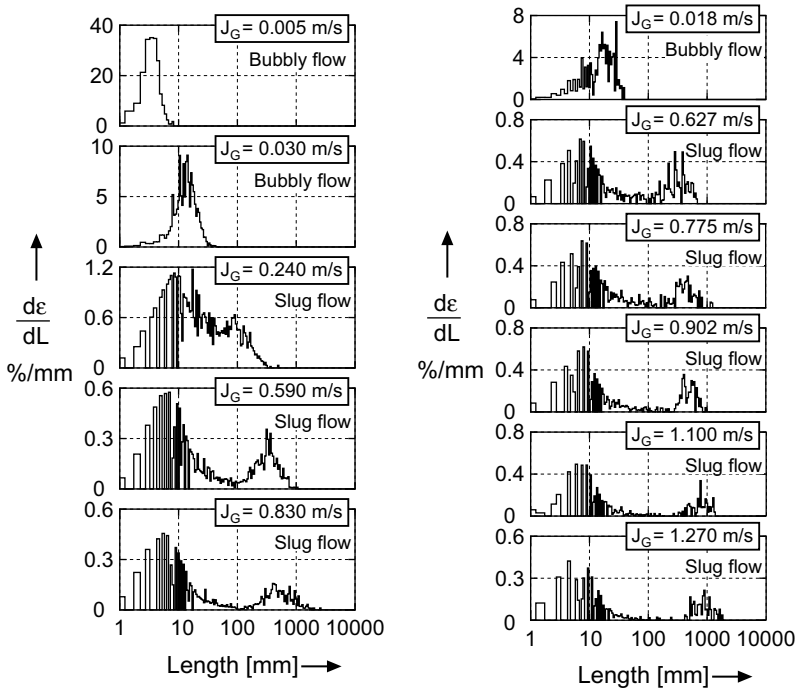

Fig. 8. Bubble length distributions for increasing gas superficial velocity J_G and constant liquid superficial velocity J_L equal to 0.11 m/s (left) and 0.14 m/s (right). The flow pattern according to the Mishima–Ishii flow map is reported for each case.

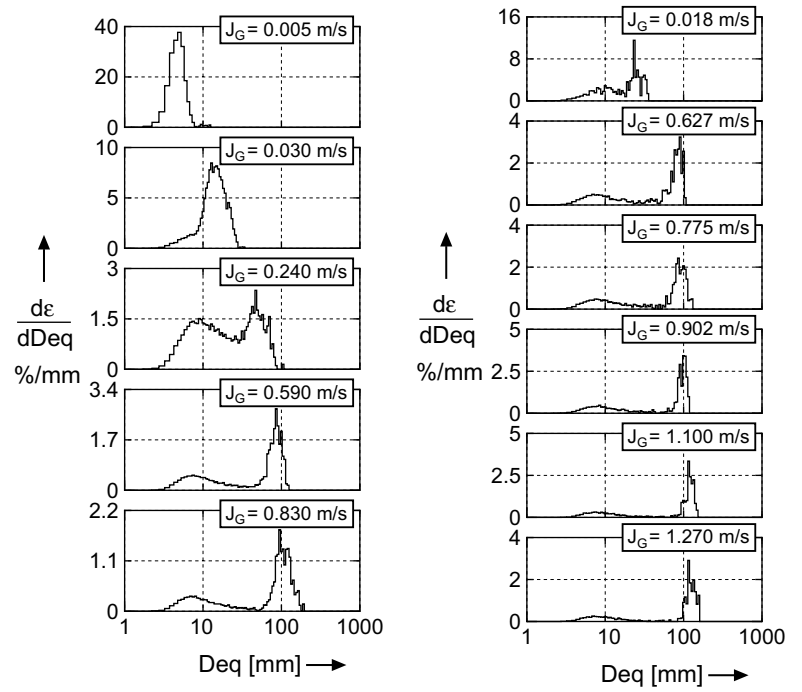

Fig. 9. Bubble equivalent diameter distributions for increasing gas superficial velocity J_G and constant liquid superficial velocity J_L equal to 0.11 m/s (left) and 0.14 m/s (right).

A method to check whether this finding holds for flashing flows as well, consists in decomposing the void-fraction radial profile in a series of partial void-fraction profiles associated to given bubble size classes. In this way it is possible to see where bubbles of a given size tend to accumulate.

Time-averaged void-fraction profiles can be obtained easily by averaging the local instantaneous void fractions ε_{ijk} over a given period (200 s in the present study). The bubble identification algorithm mentioned in Section 3.2 allows to identify the set of elements (i,j,k) belonging to a given bubble. This information can be used to decompose the void-fraction profile in partial void-fraction profiles (Prasser et al., 2002) according to bubble classes. Two bubble size classes are used for the decomposition and the critical equivalent diameter of 5.36 mm is used as threshold between the two classes.

The results of the decomposition are shown in Figs. 10 and 11 for the two sets of stationary experiments. In agreement with the findings of Tomiyama and co-workers for water–air flows (1995, 1999), small bubbles ($D < 5.36$ mm) are located preferentially close to the pipe wall, while bigger bubbles ($D \geqslant 5.36$ mm) tend to be located toward the center of the pipe. To check whether the bubble radial distribution is in equilibrium with the forces acting on the bubbles, a model developed by Lucas et al. (2001) has been applied. The model is based on a radial balance of the forces acting on the bubbles. The radial balance is solved separately for several bubble classes and the feedback between void-fraction profile and velocity profile is taken into account as well. The forces considered in the model are:

1. Lift force: this force occurs if a particle is subjected to a shear flow. According to Zun (1980) the lift force related to the unit volume can be calculated as

$$\vec{F}_{\text{lift}} = -C_{\text{lift}}\rho_{\text{L}}(\vec{w}_{\text{G}} - \vec{w}_{\text{L}}) \times \text{rot}(\vec{w}_{\text{L}}) \tag{11}$$

For a spherical bubble in an upwards pipe flow the coefficient C_{lift} is positive and the force acts toward the pipe wall. Tomiyama et al. (1995) found the force acting toward the pipe center for large, non-spherical

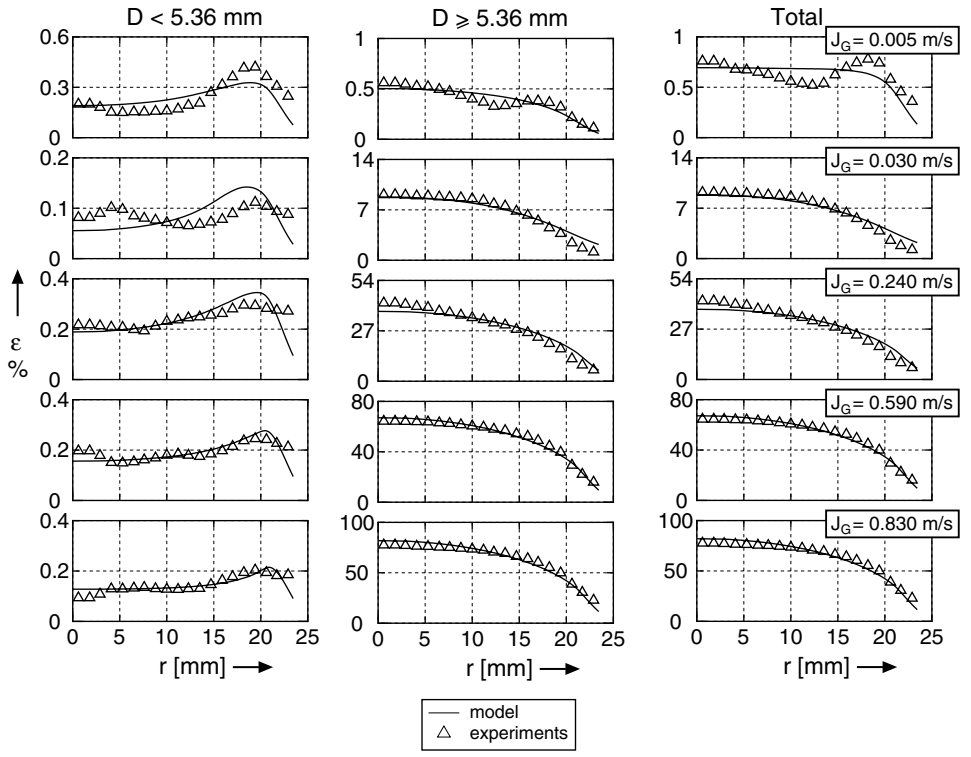

Fig. 10. Decomposition of void-fraction radial profile in two bubble size classes ($J_{\text{L}} = 0.11$ m/s). Experimental results and model predictions.

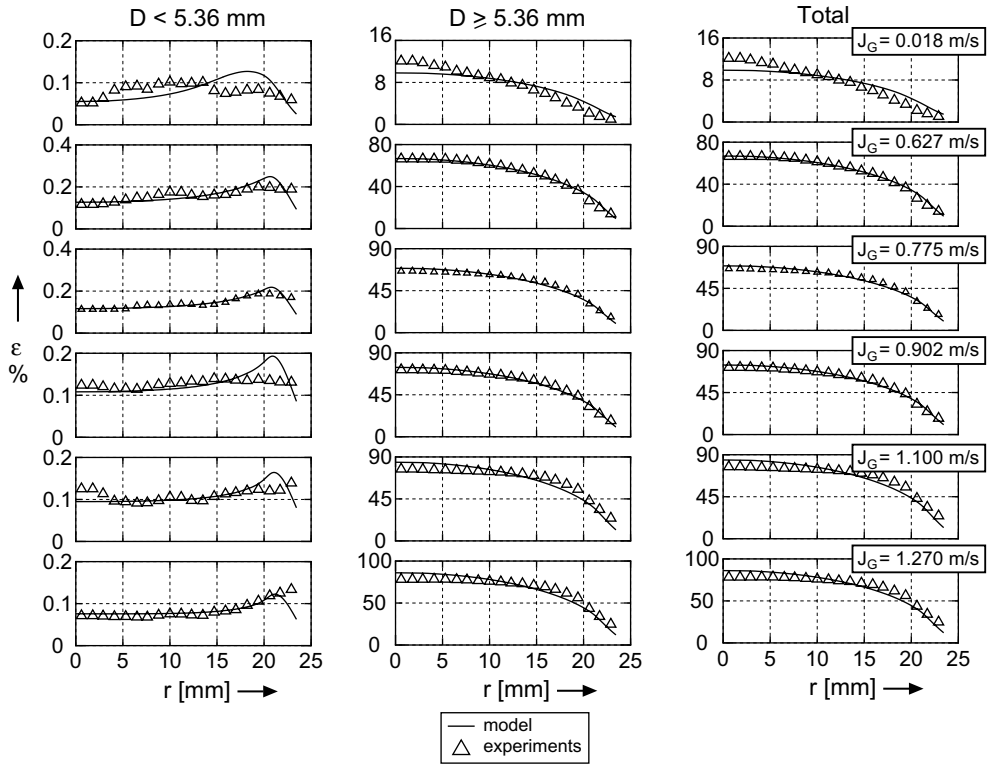

Fig. 11. Decomposition of void-fraction radial profile in two bubble size classes ($J_L = 0.14$ m/s). Experimental results and model predictions.

bubbles. Based on experimental data they developed a correlation for the coefficient of the lift force C_{lift}, which depends on the modified Eötvös number (see Eq. (10)). It changes sign at the previously mentioned critical modified Eötvös number. The correlation is used in the model.

2. Lubrication force: it was introduced by Antal et al. (1991) and is responsible for driving the bubbles away from the pipe wall. A modified expression for this force by Tomiyama et al. (1995) is implemented in the model.
3. Turbulence dispersion force: it takes into account the smoothing of the void-fraction profiles caused by turbulence (Lahey et al., 1993).
4. Eötvös number dependent dispersion force: this force has been introduced by Lucas et al. (2001) to take into account that the fluctuating motions of large bubbles ($Eo > 1$) caused by bubbles deformation produce an additional smoothing of the void-fraction profiles.

It is assumed that the forces acting on the bubble are in equilibrium. The radial profile of the liquid velocity, which is required for the calculation of the lift force, is obtained using the model from Sato et al. (1981). They consider the inherent wall turbulence as well as the turbulence caused by the bubbles. This sub-model needs the radial void-fraction profile as an input. For this reason, the radial profile of the liquid velocity and the radial profile of the gas fraction are calculated iteratively. There is a strong feedback between the two profiles.

The model allows the prediction of radial bubble distributions in a vertical two-phase flow once bubble size distributions are provided. The experimental bubble size distributions shown in Fig. 9 are given as input to the model and calculations are performed using 50 bubble classes and 100 radial nodes. To compare the results with the experimental data, the 50 bubble classes are reduced to two bubbles classes separated by the threshold defined by the equivalent critical diameter of 5.36 mm. For the reduction, it is sufficient to sum all the partial profiles of the bubble classes that have to be condensed together.

The model, successfully applied to air–water flows, is used here for the first time to study steam/water flow and no tuning of the original model in (Lucas et al., 2001) has been performed to match the experimental results presented in this work.

The comparison with the experimental void-fraction profiles is shown in Figs. 10 and 11. Fair agreement is found for the two bubble classes considered (with diameter respectively smaller and larger than the critical diameter) in correspondence of which Tomiyama et al. (1995) predict an inversion of the direction of the lift force. In particular, a wall-peaked void-fraction profile is found for small bubbles and a center-peaked profile is found for large bubbles, in agreement with the experimental results. This finding suggests that the equilibrium of forces acting on the bubbles is established fast enough in radial direction (perpendicularly to the flow), so that the equilibrium model is in good agreement with the measured results even for a flow not fully developed in axial direction (strictly speaking it is not possible to define a development length for flashing flow because bubbles are created along the entire length of the adiabatic section above the flashing front).

At low superficial steam velocities, close to the wall, a slight over-estimation of the void-fraction profile is found for large bubbles. This may be caused by a too large dispersion force. For the small bubbles the general trend is predicted reasonably well, though there are some deviations on the absolute values of the void fractions. Such deviations are in any case very small in terms of absolute void fraction and fall in the range of measurements error of the wire-mesh sensor (around 1%).

6. Transient flashing flow during flashing-induced flow oscillations in natural circulation conditions

Under specific conditions of power and inlet subcooling, flashing-induced flow-oscillations can be observed (Manera and van der Hagen, 2003). Flashing taking place in the adiabatic section of the loop leads to an unbalance between the driving force and the pressure drops in the loop, giving rise to a flow-rate increase. This will cause a decrease of the temperature at the outlet of the heated section. Thus, colder water will enter the adiabatic section suppressing flashing. When flashing stops the driving force becomes small, yielding a low flow rate. This in turn will give a subsequent increase of the fluid temperature at the inlet of the adiabatic section. Eventually, a new flashing cycle will start. In this way so-called flashing-induced flow oscillations originate.

The evolution of the flow pattern and of the bubble size distribution during a typical flashing-induced flow oscillation is discussed in the next paragraphs. For this scope, the flow pattern visualization described in Section 4 is for the first time applied to time-dependent velocity.

The first problem to be solved is to derive a time-dependent steam bubbles velocity. No literature has been found with regards to this problem (the studies published in the field mainly refer to stationary two-phase flows).

6.1. Time-dependent bubble velocity measurements

To evaluate the bubble velocity, being the superficial steam velocity unknown, the following methods can be applied:

(a) by cross-correlating the cross-sectional-averaged void fractions measured by the two wire-mesh sensors. The application of cross-correlation techniques is straight-forward, but the method leads to an approximated result since it is necessary to assume that all bubbles present in a given time interval have the same velocities;
(b) by using a drift-flux model. The GE-Ramp model (IAEA, 2001) is selected. This has been proven to give the best results in case of flashing flow (Manera et al., 2003);
(c) by identifying the time delay that it takes for each bubble to touch the two sensors. The direct identification of time delays would give the possibility of associating to each bubble its "true" velocity, identified as the velocity of the bubble front. In the case presented in Fig. 5, for example, it is clear that the velocities of the two shown bubbles significantly differ from each other. Unfortunately, if this method is performed via a computer algorithm, extreme care has to be taken for the choice of the selection conditions used to find the same bubble in the data arrays measured by the two wire-mesh sensors. This task

becomes particularly difficult in presence of high bubble density and bubble coalescence, break-up and expansion. A visualization program has been developed to allow the user to manually select and associate bubbles passing through the two wire-mesh sensors. Once the same bubble is identified in the three-dimensional data arrays delivered by the two wire-mesh sensors, the velocity of the bubble is evaluated on the basis of the time instants at which the bubble front touches successively the two sensors. This method is taken as reference for further comparisons.

To apply the cross-correlation method (a), the cross-correlation function (CCF) has to be calculated over a limited time window if the temporal variations of the steam velocity have to be derived. It is recommendable that the steam velocity is evaluated with a time step not larger than 0.5–1 s (the frequency of void fluctuations during flashing is around 3–4 Hz. The period of the flow-rate transient is ~40 s in the case presented here). The same limitation holds for the time window over which the cross-correlation is performed. Unfortunately, a small time window goes at the expenses of the accuracy of the CCF. To overcome this problem and reduce the uncertainty on the estimation of the steam velocity a second method based on ensemble-averaged CCF is applied. First, a longer measurement is performed (600 s) in comparison with the stationary measurements in order to record a significant number of flashing cycles. Then individual flashing cycles are discriminated on the basis of the signal of the lower wire-mesh sensor. The beginning of a flashing cycle is determined as the time instant at which the wire-mesh sensor measures a cross-section-averaged void fraction of at least 10%. The instantaneous cross-section-averaged void fractions measured by the two wire-mesh sensors are cross-correlated with a time step of 0.5 s. Ensemble averaging is performed over all flashing cycles in order to guarantee sufficient statistical accuracy. The steam velocity is calculated on the basis of the ensemble-averaged cross-correlation with a time step of 0.5 s. Ensemble averaging is also done for the liquid velocity and for the void fraction, in order to obtain a representative time-dependent flashing cycle. Details on the ensemble averaging technique are given in Manera (2003) and Manera et al. (2003).

The error on the steam velocity depends on the error on the traveling time of steam bubbles between the two wire-mesh sensors. This error has two components, one due to the time resolution of the cross-correlation (i.e. the sampling time equal to 1/1200 s), which causes an error of less than 4% in the range of steam velocities encountered in the experiment, and a second component caused by noise of the signal. Since the signals are strongly correlated, this error source is negligible.

For the application of method (b), the GE-Ramp model has been selected. This drift-flux model allows to calculate the steam velocity on the basis of the cross-section-averaged void fraction. As for the cross-correlation technique, it can be chosen to derive a time-dependent steam velocity for the first flashing cycle (for which the reference measurement "c" holds) or for the ensemble-averaged flashing cycle. In the latter case the ensemble-averaged void fraction has to be filled in the drift-flux model.

The comparison between the steam velocity estimations is presented in Fig. 12. The upper figure shows the performance of the cross-correlation technique applied to the first flashing cycle (CCF) and of the ensemble-averaged cross-correlation technique (ensemble CCF). The dots (reference) have been obtained applying the method (c) described previously. The general trend of the time-dependent steam velocity is caught fairly well by both methods. As expected, the first method catches better the velocity fluctuations, while the second method delivers a smoother velocity distribution.

In the lower graph the performance of the selected drift-flux model is shown. The curve "Ge-ramp" has been obtained on the basis of the time-dependent cross-section-averaged void fraction measured during the first flashing cycle, while the curve "ensemble Ge-ramp" has been obtained on the basis of the ensemble-averaged void fraction over all the measured flashing cycles. The predictions of the drift-flux model are quite satisfactory. The bubble velocity is over-estimated at the beginning and at the end of the flashing cycle, when only small bubbles are present in the flow.

6.2. Temporal evolution of bubble-size distributions

For the study of the temporal evolution of bubble size distributions and for the flow visualization, the steam velocity derived by the ensemble-averaged cross-correlation technique is used. The transient working point for the ensemble-averaged flashing cycle of the case considered is reported in Fig. 13 in the J_L–J_G phase space.

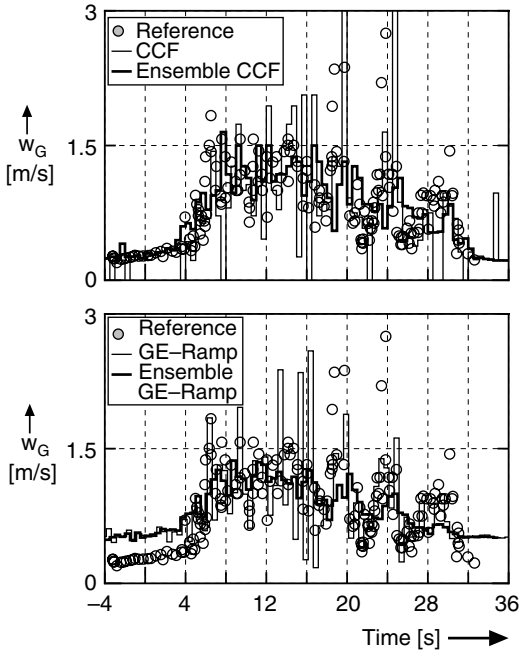

Fig. 12. Comparison between steam velocity estimations.

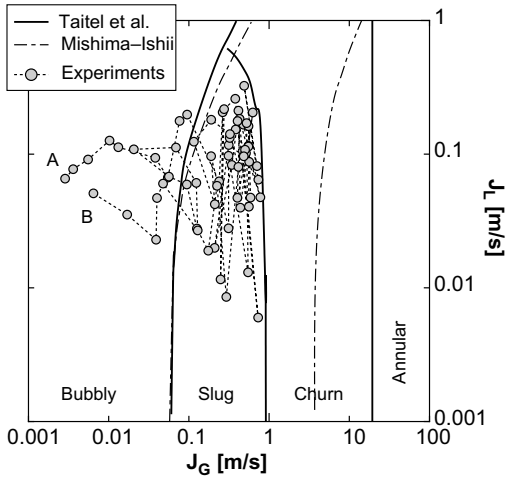

Fig. 13. Localization of transient working point in the J_L–J_G flow map. The time increases from point A to point B.

The time increases from points A (0.25 s in the time axis of Fig. 12) to B (32.25 s). The flow maps according to Taitel et al. (1980) and Mishima and Ishii (1984) are reported as well in the figure. As it can be seen, during a flashing cycle, the flow-pattern transits from bubbly-flow to slug/churn flow (between 4.25 and 4.75 s) and ends as bubbly flow again (between 29.75 and 30.25 s). This can be also seen by visual inspection of the test section and by bubbles reconstruction and flow pattern visualization, as it is demonstrated in Figs. 14 and 15.

In Fig. 14 the bubble size distributions are shown at different time instants (namely, the bubble length distributions and the bubble diameter D_{xy} distributions are presented. D_{xy} is defined as the maximum bubble diameter in the pipe cross-section). For each distribution all the bubbles found in a time interval of 4 s are

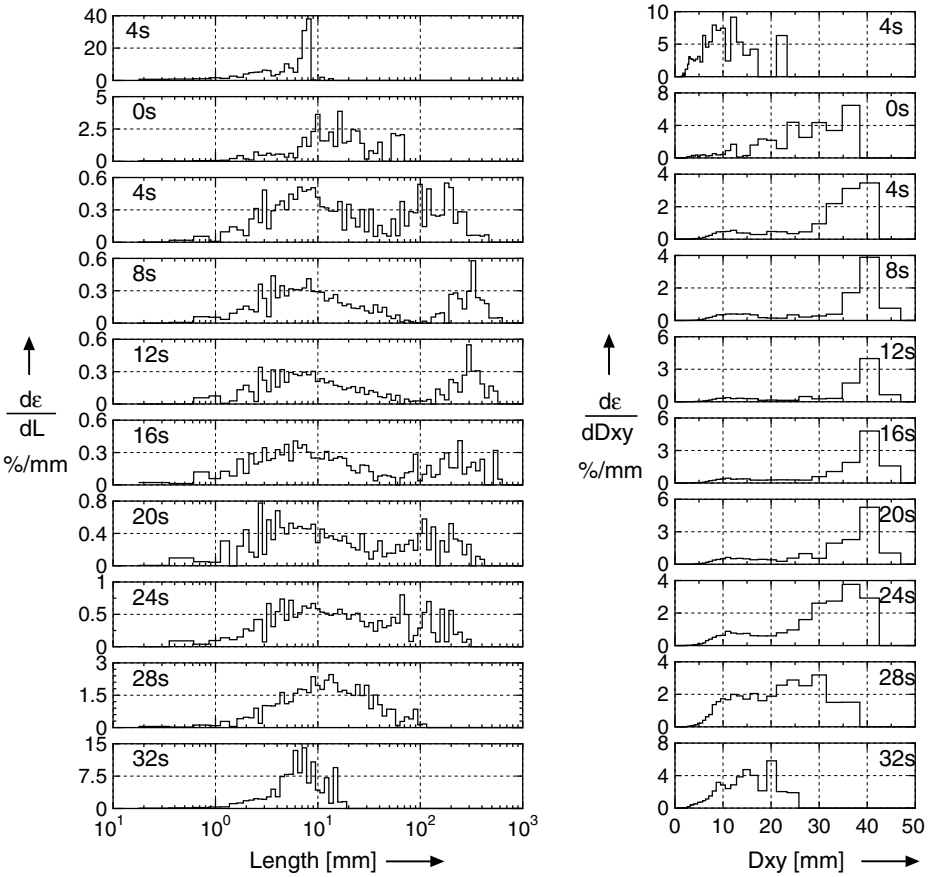

Fig. 14. Temporal evolution of bubbles length and diameter during a flashing-induced flow oscillation.

considered. All flashing cycles in the 600 s measurement are taken into account. This is possible thanks to the fact that, with the synchronisation technique described previously, a common time axis can be defined for all flashing cycles. This common time axis has been used in Fig. 12 as well.

As for the stationary case, the transition from spherical to cap bubbles is characterized by a unimodal distribution tailed toward lower bubble sizes. During the transition from cap bubbles to slug flow the unimodal distribution becomes symmetric but with a very large spreading in bubbles length. When the transition is completed the bimodal distribution typical of slug flow is found. Initially, the length of the Taylor bubbles gradually increases with time. The production of steam causes an increase of the buoyancy in the loop and consequently an increase of the liquid superficial velocity. Subsequently the length of the Taylor bubbles decreases until bubbly flow is reached again and the bubbles length distribution switches back again to unimodal. Similar conclusions can be drawn looking at the evolution of the maximum bubbles diameter D_{xy} in the cross-section (note that this quantity can be measured exactly in the limits of the wire-mesh sensor spatial resolution and it is not biased by errors in the bubbles velocity measurement).

The flow visualization at different time instants for one of the flashing cycles of the considered case is shown in Fig. 15. Two successive columns correspond to the measurements performed by the two wire-mesh sensors respectively. The picture is in scale, the length of the column being 20 times the pipe diameter ($20 * 47 = 940$ mm). The time instants corresponding to the beginning and the end of different columns are indicated for each column separately (again the same time axis as in Figs. 12 and 14 is used).

Note that if the "correct" bubble velocity is used for each bubble in the flow-pattern visualization, the distance between the bubble fronts of a given bubble as seen from the two wire-mesh sensors should be exactly equal to the distance of 27.5 mm existing between the two sensors (the distance between the two wire-mesh

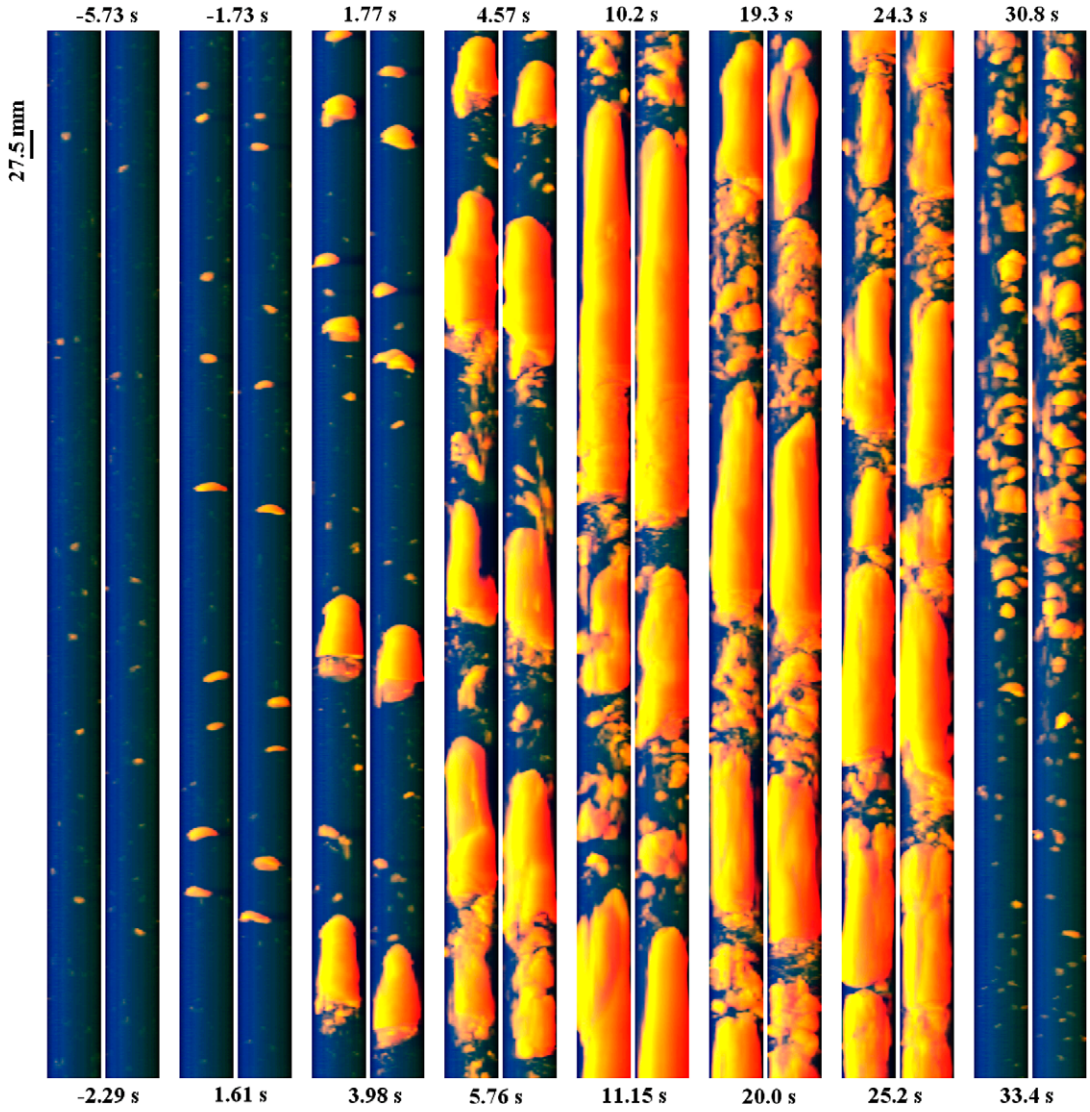

Fig. 15. Flow pattern visualization reconstructed from wire-mesh data for transient flashing flow.

sensors is reported in scale in Fig. 15). Thus, a larger or smaller distance gives an idea of the velocity under-estimation or over-estimation respectively that is caused by the use of an approximate velocity.

As mentioned previously, on the basis of the flow map presented in Fig. 13 and from visual inspection of the test section, the flow pattern transits from bubbly to slug/churn flow and back to bubbly flow in the last instants of the flashing cycle.

The flow patterns agree quite well with the prediction of the Mishima–Ishii flow maps even in transient conditions. It is important to recall that in such conditions, not only the steam is generated along the adiabatic section, but also the flashing front changes location with time. Moreover, it has to be pointed out that also the time instants at which the flow pattern transitions occurs agree quite well with the flow map shown in Fig. 13 (between 4.25 and 4.75 s for the bubbly to slug flow transition and between 29.75 and 30.25 s for the slug to bubbly flow transition). This is remarkable in view of the fact that flow maps are meant for stationary developed flows, and also because in Fig. 13 the ensemble-averaged flashing cycle is considered, while the visualization in Fig. 15 obviously shows a single flashing cycle.

7. Conclusions

The three-dimensional characteristics of flashing flow in a vertical pipe have been studied for the first time in stationary and transient conditions (during so-called flashing-induced flow oscillations). Advanced instrumentation, namely wire-mesh sensors, has been used for detailed void-fraction and steam velocity measurements. Appropriate treatment of the data delivered by the wire-mesh sensor allows a full reconstruction of the three-dimensional flow pattern visualization and helps revealing the structure of the flashing flow. Bubble size distributions have been obtained both in stationary and transient conditions.

The stationary bubbles size distributions have been used as input for a stationary model that calculates radial void-fraction profiles assuming equilibrium between the forces acting on the bubbles. The partial void-fraction profiles calculated for different bubble size classes have been compared with the experimental profiles and fair agreement has been found. This finding suggests that equilibrium in the radial direction (i.e. perpendicularly to the flow direction) is reached fast enough, so that good agreement is found between experimental radial bubbles distributions and the equilibrium model.

For the transient flashing flow different methods have been proposed to evaluate the time-dependent steam velocity. These methods are based on cross-correlation techniques and on the use of drift-flux models. Methods based on ensemble-averaging techniques considering several flashing cycles have been applied. Reasonable agreement is found when comparing the proposed methods to the actual bubble velocities.

Acknowledgment

This work has been partially sponsored within the EU Framework Program, NACUSP project, FIKS-CT2000-00041.

References

Analythis, G.T.H., Lübbesmeyer, D., 2002. Pre-test calculations on flashing-induced instability experiments in PANDA with TRAC-BF1/v2001.2 and RELAP5/MOD3.3./beta. EU project NACUSP, FIKS-CT-2000-00041, D09c.

Andersen, J.G.M., Inada, F., Klebanov, L.A., 1995. TRACG Analyses of Flashing Instability During Start-up. In: Proc. of 3rd Int. Conf. on Nucl. Eng. ICONE-3, April 23–27, Kyoto, Japan.

Antal, S.P., Lahey, R.T., Flaherty, J.E., 1991. Analysis of phase distribution in fully developed laminar bubbly two-phase flow. Int. J. Multiphase Flow 7, 635–652.

Aritomi, M., Chiang, J.H., Nakahashi, T., Watarum, M., Mori, M., 1992. Fundamental study on thermo-hydraulics during start-up in natural circulation boiling water reactors (I). J. Nucl. Sci. Technol. 29, 631–641.

Cheng, H., Hills, J.H., Azzopardi, B.J., 1998a. A study of the bubble-to-slug transition in vertical gas–liquid flow in columns of different diameter. Int. J. Multiphase Flow 3, 431.

Cheng, H.S., Khan, H.J., Rohatgi, U.S., 1998b. Simulation of SBWR startup transient and stability, BNL-65535.

Cheung, Y.K., Rao, A.S., 2000. Startup simulation of a natural circulation plant—ESBWR. In: Proc. of 8th Int. Conf. on Nucl. Eng., ICONE-8, April 2–6, Baltimore, MD, USA.

Costigan, G., Whalley, P.B., 1997. Slug flow regime identification from dynamic void fraction measurements in vertical air–water flows. Int. J. Multiphase Flow 23, 263.

Domnick, J., Durst, F., 1995. Measurement of bubble size, velocity and concentration in flashing flow behind a sudden constriction. Int. J. Multiphase flow 21, 1047–1062.

Downar-Zapolski, P., Biliki, Z., Bolle, L., Franco, J., 1996. The non-equilibrium relaxation model for one-dimensional flashing liquid flow. Int. J. Multiphase flow 22, 473–483.

Elias, E., Chambrè, P.L., 2000. Bubble transport in flashing flow. Int. J. Multiphase flow 26, 191–206.

Furuya, M., Inada, F., Yasuo, A., 1995. A Study on thermal hydraulic instability of a boiling natural circulation loop with a chimney (Part II. Experimental approach to clarify the flow instability in detail). Heat Transfer—Jpn. Res. 24, 577.

Hahne, E., Barthau, G., 2000. Evaporation waves in flashing processes. Int. J. Multiphase flow 26, 531–547.

Hills, J.H., Cheng, H., Azzopardi, B.J., 1998. Void fraction waves in vertical gas–liquid flow in a 150 mm tube. In: Proc. 3rd Int. Conf. on Multiphase Flow, ICMF '98, June 8–12, Lyon, France.

Inada, F., Furuya, M., Yasuo, A., 2000. Thermo-hydraulic instability of boiling natural circulation loop induced by flashing (analytical consideration). Nucl. Eng. Des. 200, 187–199.

IAEA, 2001. Thermal-hydraulic relationships for advanced water cooled reactors, IAEA-TECDOC-1203.

Lahey, R.T., Lopez de bertodano, M., Jones, O.C., 1993. Phase distribution in complex geometry conduits. Nucl. Eng. Des. 141, 177–201.

Lucas, D., Krepper, E., Prasser, H.-M., 2001. Prediction of radial gas profiles in vertical pipe flow on the basis of bubble size distribution. Int. J. Therm. Sci. 40, 217–225.

Manera, A., 2003. Experimental and analytical investigations on flashing-induced instabilities in natural circulation two-phase systems. Ph.D. thesis, Delft University of Technology.

Manera, A., Prasser, H.-M., van der Hagen, T.H.J.J., 2003. Assessment of void-fraction correlations and drift-flux models applied to stationary and transient flashing flow in a vertical pipe. In: Proc. NURETH-10, October 5–9, Seoul, Korea, 2003.

Manera, A., van der Hagen, T.H.J.J., 2003. Stability of natural-circulation-cooled boiling water reactors during startup: experimental results. Nucl. Technol. 143, 77–88.

Mi, Y., Ishii, M., Tsoukalas, L.H., 2001. Investigation of vertical slug flow with advanced two-phase flow instrumentation. Nucl. Eng. Des. 204, 69.

Mishima, K., Ishii, M., 1984. Flow regime transition criteria for upward two-phase flow in vertical tubes. Int. J. Heat Mass Transfer 27, 723–737.

Nicklin, D.J., Davidson, J.F., 1962. The onset of instability in two-phase slug flows. In: Proc. Inst. Mech. Eng. Symp. Two-Phase Flow, London.

Ohnuki, A., Akimoto, H., 2000. Experimental study on transition of flow pattern and phase distribution in upward air–water two-phase flow along large vertical pipe. Int. J. Multiphase Flow 26, 367.

Paniagua, J., Rothagi, U.S., Prasad, V., 1999. Modeling of thermal hydraulic instabilities in single heated channel loop during startup transients. Nucl. Eng. Des. 193, 207.

Prasser, H.-M., Böttger, A., Zschau, J., 1998. A new electrode-mesh tomograph for gas–liquid flows. Flow Meas. Instrum. 9, 111–119.

Prasser, H.-M., Scholz, D., Zippe, C., 2001. Bubble size measurements using wire-mesh sensors. Flow Meas. Instrum. 12, 299–312.

Prasser, H.-M., Krepper, E., Lucas, D., 2002. Evolution of the two-phase flow in a vertical tube—decomposition of gas fraction profiles according to bubble size classes. Int. J. Therm. Sci. 41, 17–28.

Prasser, H.-M., Misawa, M., Tiseanu, I., 2005a. Comparison between wire-mesh sensor and ultra-fast X-ray tomograph for an air–water flow in a vertical pipe. Flow Meas. Instrum. 16, 73–83.

Prasser, H.-M., Beyer, M., Böttger, A., Carl, H., Lucas, D., Schaffrath, A., Schütz, P., Weiß, F.-P., Zschau, J., 2005b. Influence of the pipe diameter on the structure of the gas–liquid interface in a vertical two-phase pipe flow. Nucl. Technol. 152, 3–22.

Richter, S., 2001. Study on multidimensional characteristics of developing bubbly flow in a rectangular channel. Ph.D. thesis, Tokyo Institute of Technology.

Riznic, J.V., Ishii, M., 1989. Bubble number density and vapour generation in flashing flow. Int. J. Heat Mass Transfer 32, 1821–1833.

Roy, R.P., Velidandla, V., Kalra, S.P., Peturaud, P., 1994. Local measurements in the two-phase region of turbulent subcooled boiling flow. Trans. ASME 116, 660.

Sato, Y., Sadatomi, M., Sekoguchi, K., 1981. Momentum and heat transfer in two-phase bubble flow—I. Int. J. Multiphase Flow 7, 167–177.

Sengstag, T., 2002. Pre-test calculations MONA-2-2 on the CIRCUS tests. EU Project, NACUSP FIKS-CT-2000-00041, report D9a.

Taitel, Y., Bornea, D., Dukler, A.E., 1980. Modelling flow pattern transitions for upward gas–liquid flow in vertical tubes. AIChE J. 26, 345–354.

Tiselj, I., Cerne, G., 2000. Some comments on the behaviour of RELAP5 numerical scheme at very small time step. Nucl. Eng. Des. 134, 3.

Tomiyama, A., 1998. Struggle with computational bubble dynamics. In: Proc. 3rd Int. Conf. on Multiphase Flow, ICMF '98, June 8–12, Lyon, France.

Tomiyama, A., Sou, A., Zun, I., Katanami, N., Sakagushi, T., 1995. Effects of Eötvös number and dimensionless liquid volumetric flux on lateral motion of a bubble in a laminar duct flow. Adv. Multiphase Flow 10, 3–15.

Tomiyama, A., Tamai, H., Shimomura, H., Hosokawa, S., 1999. Spatial evolution of developing air–water bubble flow in a vertical pipe. In: Proc. 2nd Int. Symp. on Two-Phase Flow Modelling and Experimentation, May 23–26, Pisa, Italy, vol. 2, 1027–1034.

Van Bragt, D.D.B., De Kruijf, W.J.M., Manera, A., Van der Hagen, T.H.J.J., Van Dam, H., 2002. Analytical modelling of flashing-induced instabilities in a natural circulation cooled boiling water reactor. Nucl. Eng. Des. 215, 87–98.

Van Hout, R., Barnea, D., Shemer, L., 2001. Evolution of statistical parameters of gas–liquid slug flow along vertical pipes. Int. J. Multiphase Flow 27, 1579.

Wang, G., Ching, C.Y., 2001. Measurements of multiple gas-bubble velocities in gas–liquid flows using hot-film anemometry. Exp. Fluids 31, 428–439.

Wissler, E., Isbin, H.S., Amudson, N.R., 1956. Oscillatory behavior of a two-phase natural-circulation loop. A.I.Ch.E. J. 2, 157–162.

Zun, I., 1980. The transverse migration of bubbles influenced by walls in vertical bubbly flow. Int. J. Multiphase Flow 6, 583–588.